

Selective removal of sodium ions from greenhouse drainage water – A combined experimental and theoretical approach

Qian, Zexin; Miedema, Henk; Pintossi, Diego; Ouma, Marvin; Sudhölter, Ernst J.R.

DOI

[10.1016/j.desal.2022.115844](https://doi.org/10.1016/j.desal.2022.115844)

Publication date

2022

Document Version

Final published version

Published in

Desalination

Citation (APA)

Qian, Z., Miedema, H., Pintossi, D., Ouma, M., & Sudhölter, E. J. R. (2022). Selective removal of sodium ions from greenhouse drainage water – A combined experimental and theoretical approach. *Desalination*, 536, Article 115844. <https://doi.org/10.1016/j.desal.2022.115844>

Important note

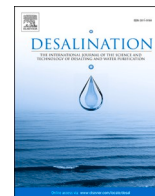
To cite this publication, please use the final published version (if applicable). Please check the document version above.

Copyright

Other than for strictly personal use, it is not permitted to download, forward or distribute the text or part of it, without the consent of the author(s) and/or copyright holder(s), unless the work is under an open content license such as Creative Commons.

Takedown policy

Please contact us and provide details if you believe this document breaches copyrights. We will remove access to the work immediately and investigate your claim.



Selective removal of sodium ions from greenhouse drainage water – A combined experimental and theoretical approach

Zexin Qian^{a,b,*}, Henk Miedema^{b,*}, Diego Pintossi^{a,c}, Marvin Ouma^b, Ernst J.R. Sudhölter^{a,d}

^a Department of Chemical Engineering, Delft University of Technology, Van der Maasweg 9, 2629 HZ Delft, the Netherlands

^b Wetsus, European Centre of Excellence for Sustainable Water Technology, Oostergoweg 9, 8911 MA Leeuwarden, the Netherlands

^c Membrane Materials and Processes, Department of Chemical Engineering and Chemistry, Eindhoven University of Technology, De Zaal, 5600 MB Eindhoven, the Netherlands

^d Faculty of Science and Technology, Membrane Science and Technology, University of Twente, Drienerlolaan 5, 7522 NB Enschede, the Netherlands

HIGHLIGHTS

- Permselectivity of the supported liquid membrane (SLM): $K^+/Na^+ = 9$, $K^+/Ca^{2+} = 15$, and $K^+/Mg^{2+} = 30$
- Simulation proved the ability of the selective removal of Na^+ by using a tandem of an in-house developed SLM and a generic CIMS.
- While maintaining Na^+ below the detrimental threshold of 4 mM, K^+ is recovered up to 96%. Water, Ca^{2+} and Mg^{2+} can be recycled up to almost 80%.

ABSTRACT

High Na^+ levels are detrimental for most crops. Selective membranes provide the possibility for the selective removal of Na^+ while preserving beneficial ion species. The challenge is to separate two ion species of the same charge. This study evaluates the implementation of an electro dialysis (ED) system equipped with a supported liquid membrane (SLM) and a commercially available monovalent cation-selective membrane (CIMS) in the treatment of greenhouse drainage water. The SLM shows a (minimum) K^+ over Na^+ , Ca^{2+} and Mg^{2+} permselectivity of 9, 15 and 30, respectively. Whereas the CIMS holds a high K^+ over Ca^{2+} and Mg^{2+} permselectivity of 10 and 16, respectively, the K^+ over Na^+ permselectivity is just 1.3. With the experimentally obtained membrane characteristics at hand, the treatment of drainage water was simulated by a two-steps process with the two membrane types operating in series. Using real-life operational parameters, analysis revealed the optimal configuration and the ability to recover 96% of the K^+ and approximately 80% of the water, Ca^{2+} and Mg^{2+} . Summarized, this study not only shows the efficient separation of two ion species of the same valance but also the implementation of this technology in a real-life application.

1. Introduction

Greenhouse horticulture has become an increasingly important method in optimizing the production of crops all year round, also in high-latitude countries, by regulating climatic conditions and efficiently making use of land, nutrients and water resources. Water quality is essential to greenhouse operation. Greenhouse irrigation normally depends on natural water sources, particularly ground or surface water. In the Netherlands, the greenhouse horticulture covers nearly 10,000 ha area, mainly in the western part of the country [1]. Compared to other Northwest European countries, both the total greenhouse area and the greenhouse density in the Netherlands are much larger [2]. However, in large parts of the Netherlands, ground and surface water quality does not meet the chemical and ecological standards as indicated by the EU Water Framework Directive [3]. Series of regulations have been released

and implemented for improving water quality in greenhouse areas, with the controllable obligations for greenhouse growers for collection and reuse of drainage water and the permission to discharge drainage water only if crop-specific sodium (Na^+) levels in drain water are exceeded or in case of emergencies (*i.e.* outbreak of diseases) [2,4–7]. To further tackle the problem of drainage water quality, agreements were made between authorities and the growers' organization targeting (nearly) zero discharge regarding nutrients and plant protection products to surface waters in 2027.

In greenhouse cultivation, nutrients and water are supplied continuously to the irrigation water system to compensate for nutrient uptake by the plants and water loss due to evapotranspiration. A high Na^+ levels (*i.e.*, above the crop specific tolerance level) is one of the detrimental factors of irrigation water quality, as it inhibits plant growth directly or indirectly by hampering the uptake of other nutrients [8–11]. Due to its

* Corresponding authors at: Wetsus, European Centre of Excellence for Sustainable Water Technology, Oostergoweg 9, 8911 MA Leeuwarden, the Netherlands.
E-mail address: zexin.qian@hotmail.com (Z. Qian).

<https://doi.org/10.1016/j.desal.2022.115844>

Received 7 February 2022; Received in revised form 3 May 2022; Accepted 4 May 2022

Available online 18 May 2022

0011-9164/© 2022 The Authors. Published by Elsevier B.V. This is an open access article under the CC BY license (<http://creativecommons.org/licenses/by/4.0/>).

low uptake by plants, Na^+ is a typical example of an ion that builds up its concentration in the irrigation water over time [12]. Therefore, desalination is becoming an attractive method for the greenhouse drainage water treatment. Reverse osmosis (RO) belongs to one of the most widely used and most cost-effective desalination technologies [13]. RO is a membrane-based, pressure-driven process that employs size exclusion to effectively reject particles and ions including Na^+ and Cl^- to produce pure water [14]. While RO yields nearly pure water with a low concentration of ions, it also rejects other ions present, for instance K^+ , Ca^{2+} , Mg^{2+} and SO_4^{2-} , all essential nutrients for crop growth [15,16]. This points to the need for ion-selective permeation approaches.

Electrodialysis (ED) is a membrane-based desalination processes using ion-exchange membranes (IEMs) and an electric field to drive the separation of the ions from the feed stream. Compared to RO, advantages of ED include high water recovery rates, long lifetime performance in desalination processes due to higher chemical and mechanical stability, less membrane fouling or scaling due to its process reversal operation, less raw water pretreatment and easier ways to adjust the separation process [17–19]. A large number of applications for ED can be found in industrial wastewater treatment [20], food and pharmaceutical industrial water treatments [21,22], portable water supply [23] and sea water desalination [24,25]. Preferential ion separation with selective IEMs for the separation of monovalent from divalent or multivalent ions has been reported [26–28]. The idea of partial desalination of the drainage water was recently proposed by monovalent ion-selective ED process for the separation of monovalent cations and divalent cations to reduce the need for adding Ca^{2+} , Mg^{2+} and SO_4^{2-} fertilizers [29]. However, it is still highly challenging to separate effectively and selectively two ionic species that share the same valence and have similar chemical properties. Within the context of greenhouse drainage water treatment, the separation of the monovalent cations K^+ and Na^+ is of utmost importance.

A previous study from our lab reports on the selective separation of K^+ from alkali metal cations [30] and divalent cations Ca^{2+} or Mg^{2+} using a supported liquid membrane (SLM) under ED conditions. The SLM is made by filling the pores of an inert porous supporting membrane with an organic solvent containing a lipophilic salt to invoke the desired membrane selectivity between cations and anions [31–33]. Preferential separation of the ions was found to follow the order of $\text{K}^+ > \text{Na}^+ > \text{Li}^+$ for alkali cations and $\text{K}^+ > \text{Na}^+ > \text{Ca}^{2+} > \text{Mg}^{2+}$ in multi-ion mixtures. The permselectivity of the SLM relies on the difference of ion dehydration energy during the ion exchange/partitioning at the water-membrane interface. Different from the SLM, commercially available special grade monovalent cation-exchange membranes (CIMS) are dense membranes with fixed negatively charged groups to the polymeric backbone (they have typically an ion-exchange capacity about 1.5–1.8 $\text{mEq}\cdot\text{g}^{-1}$ [34,35]) and a polycation layer on top, allowing the monovalent cations predominantly to permeate [36–38].

A key challenge in working towards closed loop greenhouse irrigation is dealing with the Na^+ accumulation problem. In other words: how to selectively remove Na^+ while keeping the level of other ions high, especially the one of the nutrient ion K^+ . Membrane permselectivity refers to the preferential permeation of certain ionic species through the membrane. In the literature, membranes showing a high Na^+ over K^+ permselectivity have not been reported so far. However, by combining the SLM, which holds a high K^+ over Na^+ permselectivity, with a monovalent cation-exchange membrane (CIMS), Na^+ can be selectively removed by employing a 2-step separation process. One can imagine two scenarios. In the first scenario, the CIMS separates the monovalent Na^+ and K^+ from the divalent cations, followed by the SLM that separates K^+ from Na^+ (Fig. 1a). In the alternative, second scenario, the SLM separates K^+ from Na^+ and the divalent cation followed by the separation of Na^+ from the divalent cations by the CIMS (Fig. 1b). In this study, we, first, assessed the properties of SLM and CIMS membranes. With the membrane characteristics at hand, we simulated a system with the two membrane types in tandem schemes as shown in Fig. 1. By employing a 2-step ED process, the ability to selectively separate Na^+ from greenhouse drainage water is investigated.

2. Materials and methods

2.1. Materials and chemicals

All chemicals used were of analytical grade. The ACCUREL support (polypropylene, thickness: 100 μm , pore size: 0.1 μm) was purchased from MEMBRANA. The following ion-exchange membranes have been used: standard grade Neosepta cation-exchange membrane (CMX), standard grade Neosepta anion-exchange membrane (AMX) and Neosepta monovalent selective cation-exchange membrane (CIMS). All Neosepta membranes were purchased from Eurodia. All other chemicals were purchased from Sigma-Aldrich: the organic solvent used for impregnating the ACCUREL support, 2-nitrophenyl-n-octyl ether (NPOE); the lipophilic anion sodium tetrakis[3,5-bis(trifluoromethyl)phenyl]borate (NaBARF) and the salts, KCl , NaCl , $\text{CaCl}_2\cdot 2\text{H}_2\text{O}$, $\text{MgCl}_2\cdot 6\text{H}_2\text{O}$ and Na_2SO_4 . Greenhouse drainage water samples were provided by Van der Knaap, Wateringen, The Netherlands. The cation composition of these samples were obtained by Inductively Coupled Plasma Mass Spectrometry (ICP-MS). All greenhouse drainage water received was filtered with a membrane filter (0.45 μm) to remove all solid particles before their use in ED experiments.

2.2. Membrane preparation

All experiments involving SLMs were performed with freshly prepared membranes. The organic solvent mixture for impregnating the SLM was prepared by dissolving the NaBARF into the NPOE to a fixed

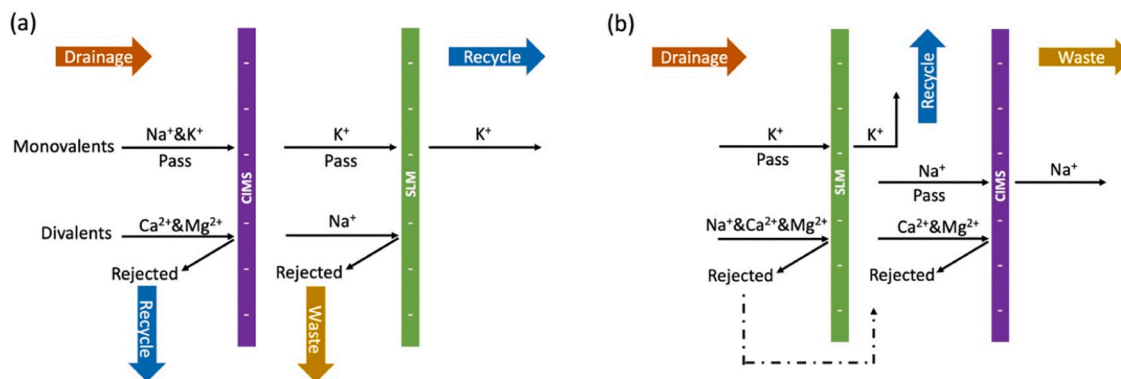


Fig. 1. Schematic outline of the two-steps treatment process with (a). a first treatment by the CIMS, followed by the SLM and (b). a first treatment by the SLM, followed by the CIMS.

concentration of 0.05 M. The porous membrane support ACCUREL was then submerged in the organic solvent mixture for 30 min at room temperature. The organic solvent quickly filled into the pores due to capillary forces.

2.3. Electrodialysis with equimolar salt solutions

Ion transport over the SLM and CIMS were first evaluated separately under ED conditions. All experiments were carried out in a six-compartment cell equipped with a platinum electrode (54 mm in diameter), as shown in Fig. 2. By using a six-compartment cell containing two Buffer compartments (compartments C), it is ensured that possible redox reactions occurring in the two outer compartments (compartments D) will not influence the composition of the ion species present in the two inner compartments (compartments A and B).

The position of cation-exchange membranes (CEM) and anion-exchange membranes (AMX) is according to the scheme shown in Fig. 2 [30]. Changes in concentration in the two inner compartments can be attributed exclusively to ion transport over the SLM or CIMS.

The SLMs and CIMS under investigation was placed into the cell with a polytetrafluoroethylene membrane holder and the effective membrane surface areas were 10 cm² in both cases. The thickness of the SLMs and CIMS are 100 μm and 150 μm, respectively. The membrane transport study was performed with the feed compartment A and receiving compartment B recirculating with an equimolar mixture of KCl, NaCl, CaCl₂ and MgCl₂ solution of which each cation concentration was 0.025 M with a total volume of 500 mL. In the two middle compartments C a buffer solution containing 0.2 M NaCl solution with the volume of 1 L was recirculated, while, an electrolyte solution containing 0.1 M Na₂SO₄ solution with a volume of 1 L was recirculated in the two outer compartments D. The flow rates in all compartments were set to 150 mL·min⁻¹. Prior to the experiments, all membranes were pre-conditioned for 24 h in the measuring solution. The temperature of all solutions was controlled at 25 ± 0.2 °C. A potentiostat (Ivium Technologies, Vertex One, Eindhoven, The Netherlands) was employed as power source for applying a constant current density. A constant current of 10 mA (corresponding to a current density of 10 A·m⁻²) was applied during a time period of 48 h. Samples of 1 mL were taken periodically during the experiment from all compartments during the experiment and the concentration of all ion species were determined using ion chromatography (IC, Metrohm compact IC 761).

2.4. Electrodialysis with greenhouse drainage water

Evaluation of the performance of the SLM and CIMS under ED conditions using the six-compartment cell was done using greenhouse drainage water provided by Van der Knaap. Table 1 shows the composition of the main cations K⁺, Na⁺, Ca²⁺ and Mg²⁺ of the received drainage water and the greenhouse stock irrigation water (stock irrigation water is pre-made high concentration irrigation water containing necessary ions and nutrients that can be diluted to the target value). In each of the compartment A and B 500 mL of this water was recirculated. In the two middle compartments C a buffer solution containing 0.05 M NaCl solution was circulated, while an electrolyte solution containing 0.05 M Na₂SO₄ solution was recirculated in compartments D. Prior to the experiments, all membranes were pre-conditioned for 24 h in the filtered greenhouse drainage water. All other experimental conditions and procedures were described in Section 2.2.

2.5. Determination of limiting current density (LCD)

Due to concentration polarization effects, the current density during ED will approach a limiting value, regardless any further increase of potential [39,40]. Operation in the so-called over-limiting current density region can cause water splitting, producing protons and hydroxide ions which serve as additional charge carriers. This needs to be avoided because it lowers the efficiency of ED regarding the ion species of interest. Therefore, the limiting current density (LCD) for both the SLM and the CIMS was determined by recording current-voltage (*i*-*V*) curves using the six-compartment cell shown in Fig. 2, with the two inner compartments filled with 0.02 M NaCl solution. The flow rate in all compartments was 150 mL/min and the membrane surface area 10 cm². While varying the current density step-wise, the potential difference between the two Haber-Luggin capillaries was measured. The *i*-*V* curves can be divided into an ohmic, a limiting and an over-limiting region [41–43], as observed in Fig. 3. The ohmic region represents a linear relation between current density and trans membrane voltage with the

Table 1
Greenhouse drainage and stock irrigation water cation composition.

Cations	K ⁺	Na ⁺	Ca ²⁺	Mg ²⁺
Drainage concentration (mM)	13	10.7	10.1	5.7
Stock irrigation concentration (mM)	9.5	0	7.0	3.0

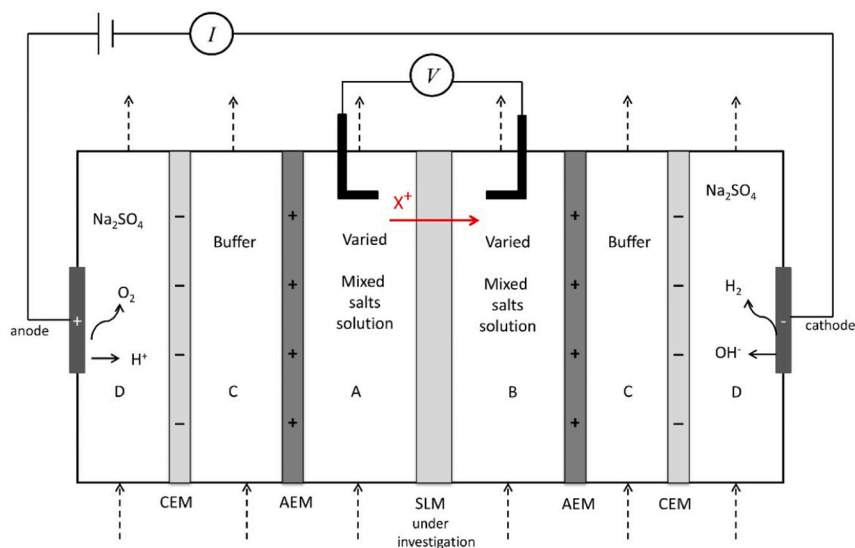


Fig. 2. Schematic view showing the configuration of the six-compartment cell used during the electro dialysis experiments. Compartments C and D as well as the position of the CEM and AEM ensure that the concentration changes in the two inner measuring compartments arise solely from ion fluxes over the SLM [30].

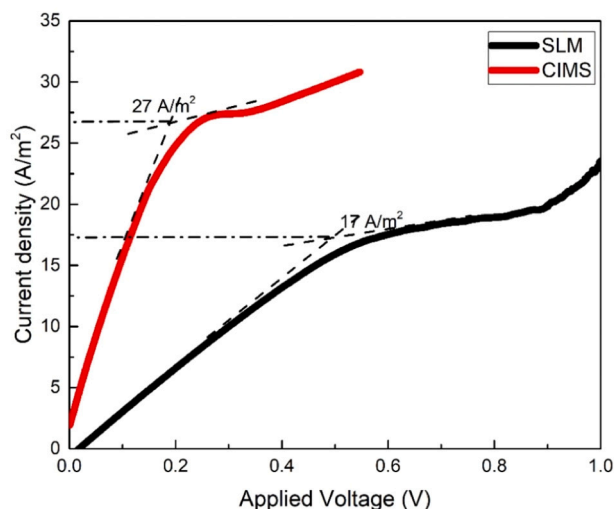


Fig. 3. i - V curves of the SLM and CIMS obtained in 0.02 M NaCl to determine the Limiting Current Density (LCD).

current increasing upon an increase of voltage. In the limiting region, the current remains constant despite an increase of voltage. Finally, in the over-limiting region the current increases again upon an increase of voltage. The LCD is defined as the current magnitude at the intersection of the extrapolated slope lines of the ohmic and limiting regions. Fig. 3 shows the i - V curves of the SLM and CIMS. The LCD value of SLM and CIMS are determined to be about $17 \text{ A}\cdot\text{m}^{-2}$ and $27 \text{ A}\cdot\text{m}^{-2}$, respectively. During the experiments as well as for the simulations, the applied current density was always set below these LCD values (see e.g. Table 2). Note that both curves do not exactly originate at zero, as expected. This deviation is most likely due to a small offset, e.g. due to liquid junction potentials, in the recorded transmembrane voltage using Haber-Luggin capillaries. Next, we briefly address the observed differences between the two curves of Fig. 3. As shown, the CIMS and SLM curves are essentially of similar shape but differ nevertheless in certain aspects. These differences, we believe, have everything to do with differences between the internal resistance of the two membranes. First, the difference in slope of the curve in the ohmic region. As discussed later on in paragraph 4.3, this reflects a difference in charge density between the

Table 2

Operational parameters employed in scenario 1 and 2, including the volumetric flow rate Q_d ($\text{m}^3\cdot\text{h}^{-1}$) of the dilute stream, applied current density I ($\text{A}\cdot\text{m}^{-2}$), ion concentration change ΔC ($\text{mol}\cdot\text{m}^{-3}$), ion transport number t of the given membrane (calculated from the equimolar mixed salt ED test) and the calculated required membrane surface area A (m^2). Note that Q_d is expressed in terms of the total volumetric flow, Q_V .

Scenario 1			
Step 1: CIMS		Step 2: SLM	
Q_d ($\text{m}^3\cdot\text{h}^{-1}$)	80% ϕ_V	Q_d ($\text{m}^3\cdot\text{h}^{-1}$)	20% ϕ_V
	1.18		0.30
I ($\text{A}\cdot\text{m}^{-2}$)	20.00	I ($\text{A}\cdot\text{m}^{-2}$)	15.00
$\Delta C_{(\text{Na}+\text{K})}$ ($\text{mol}\cdot\text{m}^{-3}$)	21.33	$\Delta C_{(\text{Na})}$ ($\text{mol}\cdot\text{m}^{-3}$)	15.63
$t_{(\text{Na}+\text{K})}$	0.70	$t_{(\text{Na})}$	0.16
A_1 (m^2)	48	A_2 (m^2)	52
Scenario 2			
Step 1: SLM		Step 2: CIMS	
Q_d ($\text{m}^3\cdot\text{h}^{-1}$)	100% ϕ_V	Q_d ($\text{m}^3\cdot\text{h}^{-1}$)	80% ϕ_V
	1.48		1.18
I ($\text{A}\cdot\text{m}^{-2}$)	15.00	I ($\text{A}\cdot\text{m}^{-2}$)	20.00
$\Delta C_{(\text{K})}$ ($\text{mol}\cdot\text{m}^{-3}$)	13.00	$\Delta C_{(\text{Na})}$ ($\text{mol}\cdot\text{m}^{-3}$)	2.55
$t_{(\text{K})}$	0.60	$t_{(\text{Na})}$	0.70
A_1 (m^2)	57	A_2 (m^2)	6

membranes. A second difference between the curves relates to the current density at which the plateau region sets in. For relatively low resistance membranes, this phenomenon generally indicates ion depletion in the feed solution at the membrane interface. However, in case of the SLM and because the curves were recorded in the same feed solution, the higher intrinsic NPOE-based membrane resistance may dominate the LCD. This effect is enhanced by the lower effective membrane surface area of the SLM because the area occupied by the ACCUREL support does not contribute at all to charge transport. Finally, the length of the plateau and the start of the over-limiting region is different. Most likely, given the low water content of the SLM, in both the CIMS and the SLM water splitting occurs in the feed boundary layer adjacent to the membrane. If correct, the moment water splitting sets in is determined by the voltage drop over the boundary layer. Assuming a similar thickness, the voltage drop over the CIMS boundary layer will be higher because of the higher current density. Because the boundary layer resistance cannot be (directly) derived from Fig. 3, further quantification is however impossible.

3. Results and discussion

3.1. Membrane characterization

3.1.1. Ion transport in equimolar salt solutions containing K^+ , Na^+ , Ca^{2+} and Mg^{2+}

To determine the membrane cation permselectivity K^+/Na^+ , $\text{K}^+/\text{Ca}^{2+}$ and $\text{K}^+/\text{Mg}^{2+}$, ED experiments with both the SLM and the CIMS were performed, in symmetrical equimolar (25 mM) solutions containing all four cation species. Fig. 4 shows the comparison between the SLM and CIMS regarding the normalized ion concentrations in feed compartment A and flux changes over a time span of 48 h. The normalized concentration is defined as the ratio of measured cation concentration at any time t and the initial cation concentration in compartment A.

As can be observed in Fig. 4a, during the first 10 h, the SLM transports preferably K^+ , with the concentrations of the other three ion species (Na^+ , Ca^{2+} and Mg^{2+}) decreasing only marginally. In all cases, the ion concentration and flux change (Fig. 4b) more or less linearly with time. Even though at a more prolonged time scale (up to 48 h), the other three ion species are transported at higher rates, K^+ transport remains dominant as reflected in the higher slope of the K^+ concentration over time. Note that the K^+ flux, as shown in Fig. 4b gradually decreases over time, from 10×10^{-6} to $6 \times 10^{-6} \text{ mol cm}^{-2} \text{ s}^{-1}$. These observations confirm previously reported data [30,44].

As anticipated, the CIMS shows a clear monovalent cation over divalent cation selectivity due to the polycation modification on the surface. Compared with the SLM, the CIMS shows much less preference of K^+ over Na^+ . Actually, over time and with the Na^+ flux gradually increasing, the difference in transport rates between K^+ and Na^+ halves over time, from an initial $1.2 \times 10^{-6} \text{ mol cm}^{-2} \text{ s}^{-1}$ at the start to $0.6 \times 10^{-6} \text{ mol cm}^{-2} \text{ s}^{-1}$ at the end of the experiment. These observations are in very close agreement with reported data in the literature [38,45].

For both the SLM and the CIMS, the summed transport numbers of all four ions are close to unity, i.e. 0.98 and 0.99, respectively, indicating that under the given experimental conditions, with an applied current density of $10 \text{ A}\cdot\text{m}^{-2}$, the current is by far predominantly carried by cations. In addition, the CIMS as well as the SLM shows a permeation preference for monovalent cations.

3.1.2. Mass and charge balance

To investigate whether the cation concentration changes in the two inner compartments of the six-compartment cell can be exclusively ascribed to transport over the central membrane mass and charge balances were set up. Theoretically, the (absolute) change of a certain cation species in each compartment should be the same in magnitude and their summation should add up to zero. Furthermore, for retaining

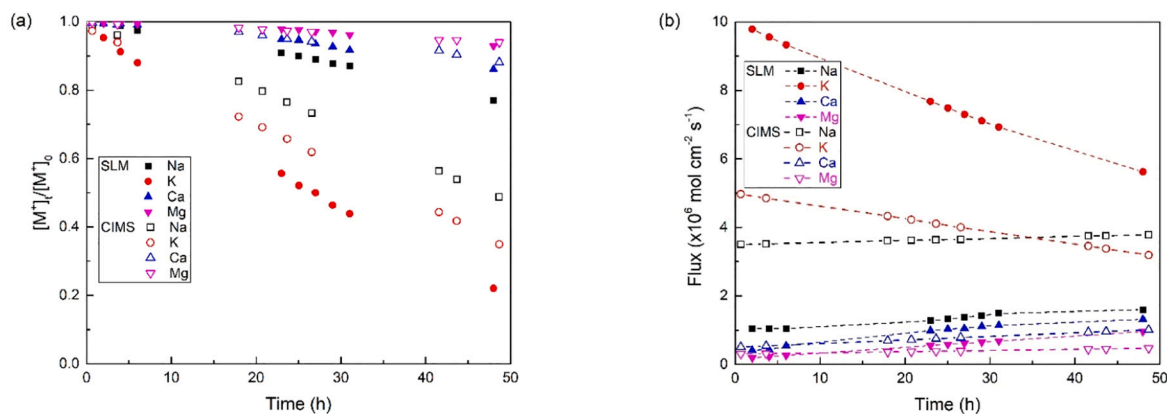


Fig. 4. Comparison between the SLM regarding (a) normalized K^+ , Na^+ , Ca^{2+} and Mg^{2+} concentration in the feed phase and (b) ion flux across the membrane. Unconnected data points refer to concentration, dotted lines to flux. Data have been obtained by experiments in equimolar (25 mM) salt solutions containing K^+ , Na^+ , Ca^{2+} and Mg^{2+} .

electro neutrality, the total charge in each compartment should also add up to zero. The mass and charge balance for the equimolar four ion mixed solutions for both the SLM and the CIMS are indeed essentially closed; detailed data can be found in the supplementary information (Table S1). The same holds for the ‘Total’ balance taking into account all six compartments. After careful evaluation, it is concluded that any deviation, *i.e.*, any non-zero value, falls in the error-range of ion concentration measurement by IC or ICP, typically $\pm 5\%$ and are not due to ion accumulation inside the membrane.

3.1.3. Permselectivity in binary salt solutions

Next, the permselectivity of the SLM and the CIMS were assessed in equimolar binary salt solutions. Following Sata [46] and Tanaka [47], the membrane permselectivity of ion species B over ion species A can be expressed as:

$$P_A^B = \frac{J_B}{J_A} \times \frac{C_A}{C_B} \quad (1)$$

where J represents the ion flux ($\text{mol} \cdot \text{m}^{-2} \cdot \text{s}^{-1}$) cross the membrane and C the ion concentration ($\text{mol} \cdot \text{L}^{-1}$) in the feed. In the current study, B represents K^+ and A represents Na^+ , Ca^{2+} or Mg^{2+} . Note that Eq. (1) represents the permselectivity, expressed in terms of fluxes, normalized for the particular ion concentrations in the feed. Fig. 5 shows the calculated membrane selectivity of the SLM and CIMS at different feed ratios, starting (at the left) from equimolar binary salt solutions, *i.e.* a feed ratio of unity.

In general, the SLM shows a rather high K^+ over Na^+ , K^+ over Ca^{2+}

and K^+ over Mg^{2+} selectivity of 9, 15 and 30, respectively, even at rather low feed concentration ratios (K^+/X^+). As anticipated, the monovalent cation over divalent cation selectivity of the CIMS is lower but still substantial, 10 and 20 for the K^+ over Ca^{2+} and K^+ over Mg^{2+} selectivity, respectively. However, the CIMS hardly discriminates between K^+ and Na^+ , reflected in a K^+ over Na^+ selectivity of just 1.3. The permselectivity of SLM mainly comes from the difference in required ion dehydration energy upon entering the membrane, thus the SLM showed good discrimination between the monovalent and divalent cations as well as between Na^+ and K^+ which have the same valence without any additional (surface) modification as present in the used commercial CIMS. In addition, the CIMS has a high IEC, leading to aggregation of the fixed anionic groups into reversed micellar structures and channels filled with water. The cations transported are therefore likely hydrated. This situation is completely different compared to the SLM, where the IEC is much lower and the anionic sites are most likely not clustered into domains. In this way it is understandable that cation dehydration energies play an important role only in SLM and not in CIMS. Both membranes share in common that the K^+ over Na^+ and K^+ over Ca^{2+} selectivity is relatively constant over the entire feed concentration ratio studied. Both membrane types differ most in respect to the K^+/Mg^{2+} selectivity. As for the SLM, though the K^+/Mg^{2+} selectivity starts high, it rapidly declines to a constant value around 30. In contrast, for the CIMS, the starting value is much lower, around 17, and remains relatively constant, gradually increases to a value around 20.

In our previous study [30,44] and from literature [48–52], we can conclude that permselectivity depends on the partitioning of the ion

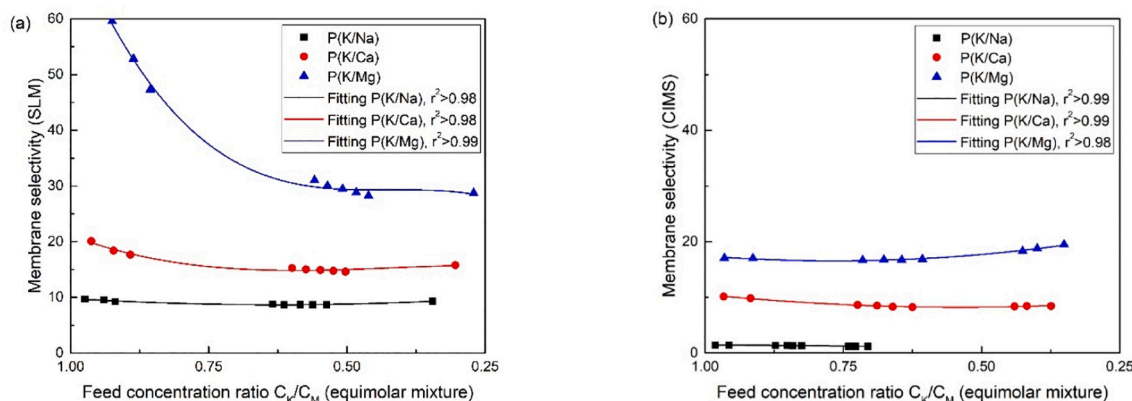


Fig. 5. Calculated membrane permselectivity $P(K/Na)$, $P(K/Ca)$ and $P(K/Mg)$ of the SLM (left) and the CIMS (right). Data has been fitted by 3rd order polynomials in order to obtain the perm selectivity at any given feed ratio, used for simulations performed later on. Data has been obtained by experiments in binary salt solutions.

species over the water and membrane phase, the ion electrophoretic mobility and the interaction between the ions and the immobile charged groups in the membrane. Ion (de)hydration plays a role in all three aspects. In partitioning, in terms of (de)hydration energy, in mobility, in terms of ion radius and in interaction, in terms of electrostatics. In case partitioning dominates, it is expected that selectivity becomes (more or less) independent of the feed concentration ratio. In the more hydrophilic CIMS [53–55], cations are less dehydrated than in the SLM. By implication, the interaction between these hydrated cations and the immobile charged moieties in the membrane is less than between the more dehydrated cations and the borate moieties in the SLM. This probably explains the different selectivity behavior in relation to the feed concentration ratio, as shown in Fig. 5. Apparently, at lower K^+/Mg^{2+} feed ratios, the interaction between Mg^{2+} and borate starts to affect the permselectivity of the SLM. Noteworthy, a feed concentration ratio-dependent selectivity is not uncommon, for example, for ion channels, membrane embedded proteins mediating the (selective) ion transport over biological membranes [56].

In terms of current density, Eq. (1) can be expressed as:

$$P_A^B = \frac{z_A I_B}{z_B I_A} \times \frac{C_A}{C_B} \quad (2)$$

where z_i and I_i (in $A\ m^{-2}$) are the charge and the current density of ion species i , respectively. Fitting the data of Fig. 4 renders the permeability of each ion species relative to that of K^+ at any given feed ratio.

The current carried by Na^+ , Ca^{2+} and Mg^{2+} and expressed in terms of I_K follows directly from Eq. (2) and is given by:

$$I_i = I_K \frac{1}{P_i^K} \frac{z_i C_i}{z_K C_K} \quad (3)$$

with i representing Na^+ , Ca^{2+} or Mg^{2+} . Ignoring the possible contribution of any other ion species (i.e., H^+ and Cl^-), the applied current density (I) in the equimolar mixed solution equals:

$$I = I_K + I_{Na} + I_{Ca} + I_{Mg} \quad (4)$$

Combining Eqs. (3) and (4) gives:

$$I_K = \frac{I_{tot}}{\left(1 + \frac{1}{P_{Na}^K} \frac{C_{Na}}{C_K} + \frac{2}{P_{Ca}^K} \frac{C_{Ca}}{C_K} + \frac{2}{P_{Mg}^K} \frac{C_{Mg}}{C_K}\right)} \quad (5)$$

The initial feed concentrations (ratios) of all four ion species are known. The data fitting of Fig. 5 renders the permselectivity of each ion species relative to that of K^+ at any given feed ratio. Using Eq. (5), I_K (at $t = 0, t_0$) can be calculated. Once I_K is known, Eq. (3) allows the calculation of the other three ion currents. Using Eq. (6), these calculated

currents serve as input to calculate the feed concentration (in M) at time t_1 after which the currents at t_1 are calculated and from that the feed concentrations at t_2 .

$$\Delta C_i = \frac{A z_i I_i \Delta t}{FV} \quad (6)$$

where F is the Faraday constant ($96,485\ C \cdot mol^{-1}$), A the (effective) membrane surface area (m^2) and V the volume of feed compartment (L). Given the initial feed composition, the applied current density, the permselectivity and transport numbers of the SLM and CIMS, this procedure simulates the ion concentration changes over time. In the next section, the same calculation will be used to simulate the treatment of (synthetic) irrigation water containing four cation species.

3.2. Transport in synthetic greenhouse drainage water

The performance of the SLM and CIMS were tested in synthetic greenhouse drainage water containing K^+ , Na^+ , Ca^{2+} and Mg^{2+} , all in concentrations as indicated in Table 1. Fig. 6 show the comparison between the experimentally obtained ion concentration changes and the simulated values based on the membrane permselectivity calculated from the equimolar binary salt solutions, as outlined in Section 3.1.3. The summed cation transport numbers for SLM and CIMS are 0.94 and 0.98, respectively, indicating that also under these given experimental condition the current is predominantly carried by cation species. As expected, with the K^+ selective SLM (Fig. 6a), K^+ was preferably being removed from the feed solution, with the concentration decreasing from 13 mM to 3.5 mM. With the monovalent cation-selective CIMS (Fig. 6b), Na^+ and K^+ were both being removed from the feed solution with a concentration decrease from 10.7 mM and 13 mM to 0.5 and 0.3 mM, respectively.

The simulations of the ion concentrations, represented as solid lines in Fig. 6, are fairly close to the experimental results for both membranes. In the case of SLM, the simulation underestimates the K^+ concentration at low feed concentration ratios. By implication and because of the constant current density applied, the concentrations of the other three ion species are slightly overestimated. Apparently, the selectivity as obtained in binary mixtures (Fig. 4) slightly deviates from the selectivity shown in mixtures containing four different cation species instead. This may not come as a surprise given the observation that even in a binary mixture selectivity depends, to a more or lesser extent, on the feed concentration ratio, notably the K^+/Mg^{2+} selectivity of the SLM.

The next step is to simulate a system with the two membrane types in series and investigate the Na^+ removal ability of such a system as well as the recovery of the three other cation species. In addition, water loss and energy consumption will be briefly discussed as well.

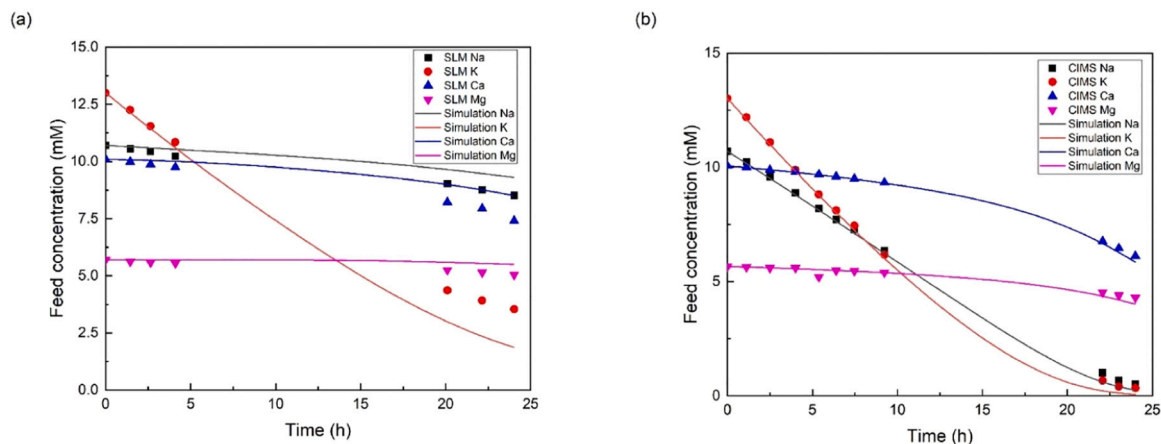


Fig. 6. Experimental (symbols) and simulated (solid lines) feed cation concentrations as obtained in synthetic greenhouse water with initial composition as presented in Table 1 and using either the SLM (left) or the CIMS (right). The simulations are based on the selectivity determined in binary salt solutions, shown in Fig. 4.

4. Implementation of the membrane-based ED system

4.1. Process design

Obviously, from a practical, experimental point of view, a membrane with a high Na^+ over K^+ selectivity would be by far the best or at least most straightforward option to selectively remove Na^+ . However, as discussed in the previous sections, our SLM shows an inverse selectivity, i.e. a high K^+ over Na^+ permselectivity. For that reason, the Na^+ separation technology to be developed is bound to a two-step process with the SLM (separating K^+) and CIMS (separating Na^+ from Ca^{2+} and Mg^{2+}) operating in two different tandem schemes shown in Fig. 1.

The tandem schemes of Fig. 1 and the two treatment scenarios of Fig. 7 show just one CIMS and one SLM membrane. One can imagine in order to scale up one can use a multi-units ED stack instead. Fig. S1 in the Supplementary Information illustrates this option schematically.

Fig. 7a outlines scenario 1 with the separation of divalent and monovalent cations using the CIMS in the first step, followed by the separation of K^+ and Na^+ using the SLM. Fig. 7b illustrates scenario 2 with the separation of Na^+ and divalent cations from K^+ using the SLM in first step, followed by the separation of Na^+ and divalent cations using the CIMS. Apart from positioning the SLM and CIMS in different order, the identity of the dilute and concentrate streams for either the SLM or the CIMS differ as well as the point where fresh irrigation water (IR) and

stock solution enters the process stream. In scenario 1, IR water and stock solution enters the greenhouse directly. The drainage water leaving the greenhouse and entering the SLM functions both as dilute and concentrate stream. In the first step of scenario 2, the dilute stream of the SLM is, as in scenario 1, made up by drainage water leaving the greenhouse. However, in this case an irrigation stock solution with the ionic composition shown in Table 1 is introduced as the concentrate stream. With the volumetric flow of dilute and concentrate stream the same, the SLM step is also the point where IR water enters the system. In scenario 1, the concentrate stream leaving the CIMS functions as the dilute stream for the SLM in step 2. In scenario 2, the concentrate leaving the SLM is directly fed back to the greenhouse. As shown in Fig. 7a, in scenario 1, the volumetric flow leaving the greenhouse (ϕ_V) is, before entering the CIMS, distributed over two streams $Q_{d,s1}$ and $Q_{c,s1}$. Later on in step 2, $Q_{c,s1}$ becomes the dilute stream for the SLM, $Q_{d,s2}$. The streams $Q_{d,s1}$ and $Q_{d,s2}$ are not independent (if, for example, $Q_{d,s1} = 20\% \phi_V$ then $Q_{d,s2} = 80\% \phi_V$), and their ratio has a direct and significant effect on the entire separation and recovery process. We therefore performed a sensitivity test to calculate the effect of the distribution ratio at point A. The (arbitrary) chosen $Q_{d,s1}/Q_{d,s2}$ ratios were 20/80, 50/50 and 80/20. As for scenario 2, here $Q_{d,s1}$ and $Q_{d,s2}$ are independent. $Q_{d,s1}$ equals the total volumetric flow leaving the greenhouse. At point B the outlet from $Q_{d,s2}$, can take any value between 0 and Q_V and with that determines for a large extent the total water loss of the system.

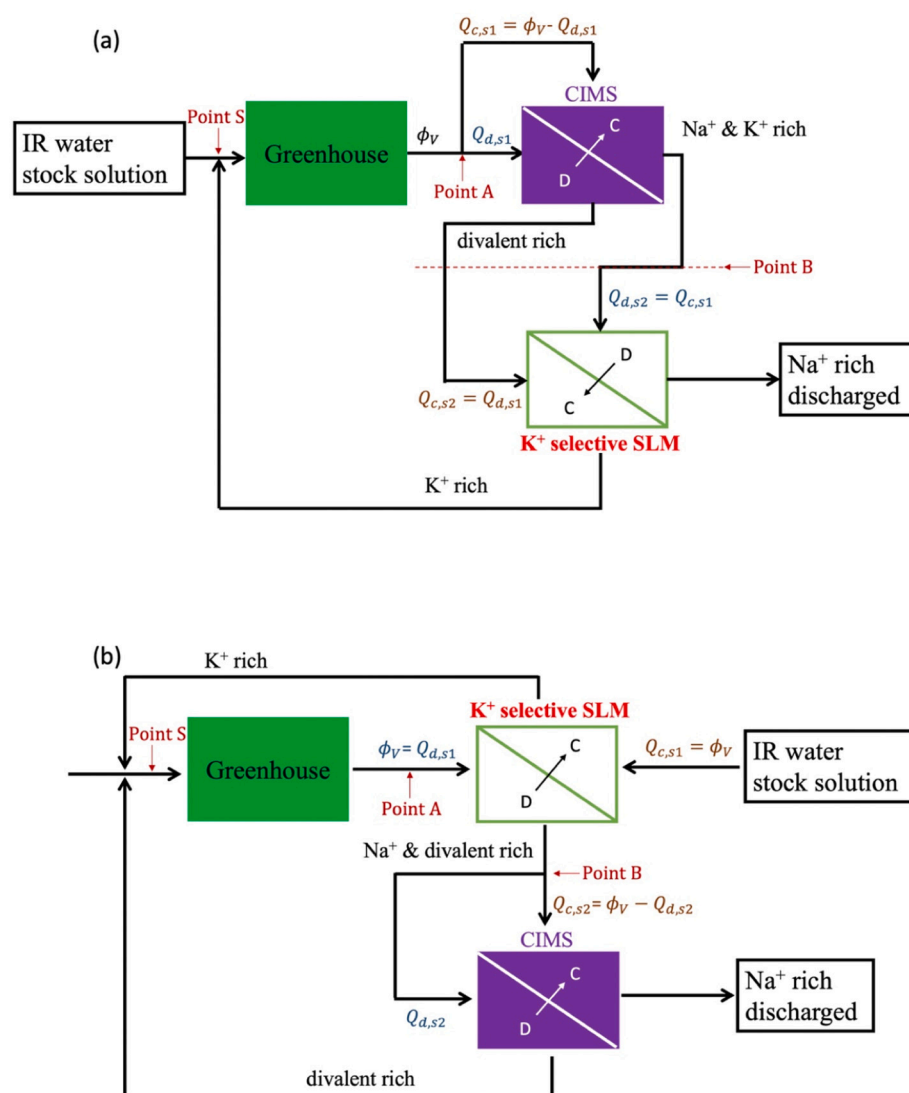


Fig. 7. Two-step treatment of greenhouse drainage water for the selective removal of Na^+ with a combination of the SLM and CIMS in ED system, (a) scenario 1 and (b) scenario 2. $Q_{d,s1}$ or $Q_{d,s2}$ indicate the volumetric flow of the dilute stream in step 1 and step 2, respectively. $Q_{c,s1}$ or $Q_{c,s2}$ indicate the volumetric flow of the concentrate stream in step 1 and step 2, respectively. D and C indicate the dilute and concentrate stream, respectively. The ionic current from D to C is composed of K^+ , in the case of the SLM, or $\text{K}^+ + \text{Na}^+$, in the case of the CIMS.

Detailed information regarding the sensitivity study and the simulation data can be found in the supplementary information (Table S2). Here we suffice by giving the final result, *i.e.*, the optimal volumetric flow rates turned out to be: $Q_{d,s1} = 80\% \Phi_V$ and $Q_{d,s2} = 20\% \Phi_V$ for scenario 1 and $Q_{d,s2} = 80\% \Phi_V$ for scenario 2.

4.2. Optimal membrane surface area and K^+ , Ca^{2+} and Mg^{2+} recovery rates

The required total membrane surface area (A) is a key operational parameter. The calculation of A requires the input of several other parameters. Eq. (7) gives the required value of A as a function of ion transport number (t_i), ion concentration difference between the dilute stream entering and leaving the membrane module ΔC_i , the applied current density I ($A \cdot m^{-2}$), the Faraday constant F ($96,485 C \cdot mol^{-1}$) and volumetric flow of the dilute through the membrane module Q_d ($m^3 \cdot h^{-1}$) [57].

$$A = \frac{Q_d \times F \times \Delta C_i}{I \times t_i} \quad (7)$$

Note that in this study Eq. (7) is exclusively used for monovalent cations, therefore the charge of the ion (+1) is not specified explicitly.

Table 2 summarizes a number of operational parameters including Q_d ($m^3 \cdot s^{-1}$), based on the sensitivity study discussed previously, I ($A \cdot m^{-2}$), based on the LCD analysis, ΔC ($mol \cdot m^{-3}$), based on greenhouse requirements, t_i , based on the experimentally obtained membrane selectivity properties and, finally, A (m^2), calculated according to Eq. (7), all for both membrane types (*i.e.*, for step 1 and step 2) and for both scenarios.

As for the ion concentration changes, two requirements were at the base of the calculation. First, the Na^+ level of the water entering the greenhouse (point S in Fig. 6) should remain below the threshold value of 4 mM. Secondly, the aim to recover as much K^+ as possible. This combined aim determines, together with the composition of the water leaving the greenhouse and the added stock solution/fresh IR water, the ΔC values for of K^+ , Na^+ and $K^+ + Na^+$. Once these ΔC values are known and together with Q_d , I_{tot} and t_i values, A can be calculated, of both the SLM and the CIMS and for both scenarios. As for scenario 1, the required membrane surface areas for the CIMS in step 1 and the SLM in step 2 turn out to be 48 m^2 and 52 m^2 , respectively. As for scenario 2, the calculated surface area of the SLM in step 1 is 57 m^2 and of the CIMS in step 2, 6 m^2 .

Note that the transport number t_i listed in Table 2 represents either the ion or the sum of the ions of choice. Given the cation selectivity of both the SLM and the CIMS, the unaccounted part of the transport number that deviates from unity represents a charge carried by divalent cations.

With the membrane surface areas calculated, all relevant parameters of the SLM and CIMS are defined. Table 3 summarizes the recovery rates of K^+ , Ca^{2+} and Mg^{2+} as well as of water. Based on these numbers, scenario 2 performs slightly better, notably regarding the recovery of Ca^{2+} and Mg^{2+} .

4.3. Outlook

Any potential real-life application of the system outlined here depends on its competitiveness with currently existing technology. The economics of the SLM-based technology, in turn, will depend (to a more

Table 3

Summary of the recovery rates of K^+ , Ca^{2+} and Mg^{2+} as well as of water when applying either scenario 1 or 2.

	Recovery			
	K^+	Ca^{2+}	Mg^{2+}	Water
Scenario 1	97%	63%	68%	80%
Scenario 2	96%	79%	79%	80%

or lesser extent) on the life-time of the SLM. In order to investigate its stability in terms of both mechanical strength and functionality, the SLM was exposed to the same experimental conditions as applied before (Table 2) but for a period of 20 days. Fig. 8 shows the ionic fluxes over the SLM in equimolar mixed salt solutions containing Na^+ , K^+ , Ca^{2+} and Mg^{2+} during 20 days of continuous operation with the solution refreshed every two days. Fig. 8 allows two conclusions. Firstly, the selectivity shown is in line with the selectivity seen in Figs. 4–6, with a selectivity order of $K^+ > Na^+ > Ca^{2+} > Mg^{2+}$. Secondly, the functionality of the SLM, regarding both selectivity and flux magnitude, remains fairly constant over the 20 days period.

Addition to the membrane lifetime, another hurdle to take on the way to application is lowering the membrane resistance of the SLM and with that the ED energy consumption. As evident from Fig. 3, for any applied current density, the recorded voltage over the membrane is higher for the SLM than for the CIMS, indicating the higher SLM resistance. A factor of 6 can be calculated from the slope from Fig. 3 between the resistance of SLM and CIMS. This is mainly due to the lower IEC of the SLM. The maximal solubility of the Na^+ borate salt used here in NPOE is 50 mM, equivalent to an IEC of 0.085 $mEq \cdot g^{-1}$. With a reported IEC of 1.5–1.8 $mEq \cdot g^{-1}$, the IEC of the CIMS is approximately 20 times higher. The difference of the observed ratio of 6 from LCDs for membrane resistance in comparison to the ratio of 20 as deduced from the IEC, likely points to differences in ionic aggregation and the formation of intimate ion-pairs between anionic charged groups and cations that has been described in literature [58]. There are essentially two ways to lower the SLM resistance. Firstly, increasing the IEC of the SLM by a different combination of salt and organic solvent. Secondly, a reduction of the membrane thickness from 100 μm , preferably to the $<10 \mu m$ range, possibly in combination with a porous support rendering the necessary mechanical strength.

5. Conclusion

As determined in binary equimolar salt solutions, the SLM shows a K^+ over Na^+ , K^+ over Ca^{2+} and K^+ over Mg^{2+} selectivity of 9, 15 and 30, respectively, even at rather low K^+ feed concentrations and low feed ratios. When extrapolated to solutions containing K^+ , Na^+ , Ca^{2+} and Mg^{2+} , these binary selectivities predict quite well the experimentally observed concentrations changes over time of all four cation species. Because the SLM demonstrates a permeation preference of K^+ over Na^+ ,

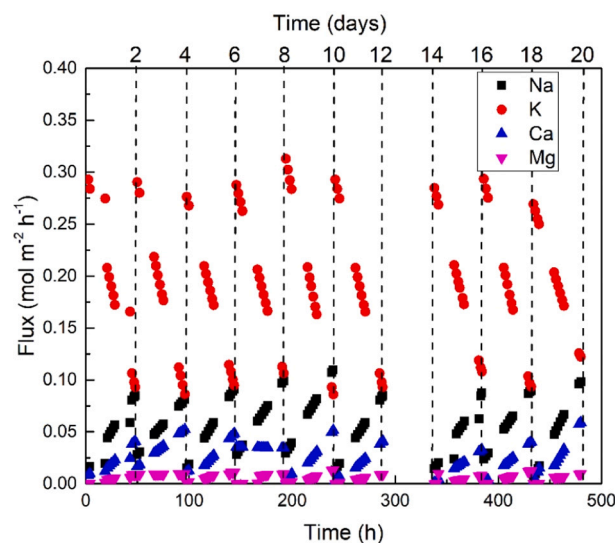


Fig. 8. SLM mediated ionic fluxes carried by Na^+ , K^+ , Ca^{2+} and Mg^{2+} under ED conditions during 20 days of continuous operation with the solution refreshed every two days.

the selective removal of Na^+ from greenhouse irrigation water requires a two-step process implying the SLM operating in series with a (generic commercially available) CIMS with a monovalent cation over divalent cation selectivity. Based on the permeation characteristics of both the SLM and the CIMS, this two-step process has been simulated using real-life operational input parameters. Starting point of the simulation was the (mandatory) requirement to keep the Na^+ concentration below its (toxic) threshold of 4 mM, while recovering as much K^+ as possible. With nearly all K^+ recovered (96%), the recovery of Ca^{2+} , Mg^{2+} and water turned out to be around 80%, indicating the efficiency of the novel tandem technology presented here.

CRedit authorship contribution statement

Zexin Qian: Conceptualization, Investigation, Formal analysis, Data curation, Writing – original draft. **Diego Pintossi:** Formal analysis (simulation model), Data curation (simulation model). **Marvin Ouma:** Data curation (SLM stability study). **Henk Miedema:** Supervision, Conceptualization, Formal analysis, Writing – review & editing. **Ernst J. R. Sudhölter:** Supervision, Conceptualization, Writing – review & editing.

Declaration of competing interest

The authors declare that they have no known competing financial interests or personal relationships that could have appeared to influence the work reported in this paper.

Acknowledgements

This work was performed in the cooperation framework of Wetsus, European Centre of Excellence for Sustainable Water Technology (www.wetsus.nl). Wetsus is co-funded by the Dutch Ministry of Economic Affairs and Ministry of Infrastructure and Environment, the European Union Regional Development Fund, the Province of Fryslan and the Northern Netherlands Provinces. This work is part of a project that has received funding from the European Union's Horizon 2020 research and innovation program under the Marie Skłodowska-Curie grant agreement No 65874. The authors like to thank the participants of the research theme “Desalination” for the fruitful discussions and their financial support. A special word of thank goes to Van der Knaap (The Netherlands) and Yara (The Netherlands) for all their advice and support.

Appendix A. Supplementary data

Supplementary data to this article can be found online at <https://doi.org/10.1016/j.desal.2022.115844>.

References

- [1] M. Raaphorst, Quantitative Information for Greenhouse Horticulture, Report GTB-5154, Wageningen, 2017.
- [2] C. van der Salm, W. Voogt, E. Beerling, J. van Ruijven, E. van Os, Minimising emissions to water bodies from NW European greenhouses; with focus on Dutch vegetable cultivation, *Agric. Water Manag.* 242 (2020), <https://doi.org/10.1016/j.agwat.2020.106398>.
- [3] EU-WFD, Water Framework Directive, Directive 2000/60/EC of the European Parliament and of the Council of 23 October 2000 establishing a framework for Community action in the field of water policy, *Off. J. Eur. Commun.* L327/1-72 (2000) http://ec.europa.eu/environment/water/water-framework/index_en.html.
- [4] G.B.K. Roos-Schalij, M.P. Leunissen, K. Krijt, Lozingenbesluit WVO Glastuinbouw, the Hague. <https://wetten.overheid.nl/BWBR0013430/2005-11-15/1>, 1994.
- [5] EU-ND, Nitrate Directive, Council Directive of 12 December 1991 concerning the protection of waters against pollution caused by nitrates from agricultural sources (91/676/EEC), *Off. J. Eur. Commun.* L 375/1-8 (1992) <https://eur-lex.europa.eu/legal-content/EN/TXT/PDF/?uri=CELEX:31991L0676&from=EN>.
- [6] Besluit Glastuinbouw, Regulation Greenhouse Horticulture. <https://wetten.overheid.nl/BWBR0013430/2012-01-01>, 2002.
- [7] E.A.M. Beerling, C. Blok, A.A. Van Der Maas, E.A. Van Os, Closing the water and nutrient cycles in soilless cultivation systems, *Acta Hortic.* 1034 (2014) 49–55. [10.17660/ActaHortic.2014.1034.4](https://doi.org/10.17660/ActaHortic.2014.1034.4).
- [8] J.L. Zhang, T.J. Flowers, S.M. Wang, Mechanisms of sodium uptake by roots of higher plants, *Plant Soil* 326 (2010) 45–60, <https://doi.org/10.1007/s11104-009-0076-0>.
- [9] A.D. Blaylock, Cooperative Extension Service Soil Salinity, Salt Tolerance, And Growth Potential of Horticultural And Landscape Plants, 1994.
- [10] A. Läuchli, S.R. Grattan, Plant growth and development under salinity stress, in: *Adv. Mol. Breed. Toward Drought Salt Toler. Crop*, Springer, Netherlands, 2007, pp. 1–32, https://doi.org/10.1007/978-1-4020-5578-2_1.
- [11] T.B. Kinraide, Interactions among Ca^{2+} , Na^+ and K^+ in salinity toxicity: quantitative resolution of multiple toxic and ameliorative effects, *J. Exp. Bot.* 50 (1999) 1495–1505, <https://doi.org/10.1093/jxb/50.338.1495>.
- [12] A.M.S. Abdol Qados, Effect of salt stress on plant growth and metabolism of bean plant *Vicia faba* (L.), *J. Saudi Soc. Agric. Sci.* 10 (2011) 7–15, <https://doi.org/10.1016/j.jssas.2010.06.002>.
- [13] S. Burn, M. Hoang, D. Zarzo, F. Olewniak, E. Campos, B. Bolto, O. Barron, Desalination techniques - a review of the opportunities for desalination in agriculture, *Desalination* 364 (2015) 2–16, <https://doi.org/10.1016/j.desal.2015.01.041>.
- [14] C. Fritzmann, J. Löwenberg, T. Wintgens, T. Melin, State-of-the-art of reverse osmosis desalination, *Desalination* 216 (2007) 1–76, <https://doi.org/10.1016/j.desal.2006.12.009>.
- [15] D. Cohen-Tanugi, J.C. Grossman, Water desalination across nanoporous graphene, *Nano Lett.* 12 (2012) 3602–3608, <https://doi.org/10.1021/nl3012853>.
- [16] U. Yermiyahu, A. Tal, A. Ben-Gal, A. Bar-Tal, J. Tarchitzky, O. Lahav, Rethinking desalinated water quality and agriculture, *Science* (80-) 318 (2007) 920–921, <https://doi.org/10.1126/science.1146339>.
- [17] H. Strathmann, Electrodialysis, a mature technology with a multitude of new applications, *Desalination* 264 (2010) 268–288, <https://doi.org/10.1016/j.desal.2010.04.069>.
- [18] T. Scarazzato, K.S. Barros, T. Benvenuti, M.A.S. Rodrigues, D.C.R. Espinosa, A.M. B. Bernardes, F.D.R. Amado, V. Pérez-Herranz, Achievements in electrodialysis processes for wastewater and water treatment, in: *Curr. Trends Futur. Dev. Membr. Elsevier*, 2020, pp. 127–160, <https://doi.org/10.1016/b978-0-12-817378-7.00005-7>.
- [19] L. Ge, B. Wu, D. Yu, A.N. Mondal, L. Hou, N.U. Afsar, Q. Li, T. Xu, J. Miao, T. Xu, Monovalent cation perm-selective membranes (MCPMs): new developments and perspectives, *Chin. J. Chem. Eng.* 25 (2017) 1606–1615, <https://doi.org/10.1016/j.cjche.2017.06.002>.
- [20] T. Benvenuti, M.A. Siqueira Rodrigues, A.M. Bernardes, J. Zoppas-Ferreira, Closing the loop in the electroplating industry by electrodialysis, *J. Clean. Prod.* 155 (2017) 130–138, <https://doi.org/10.1016/j.jclepro.2016.05.139>.
- [21] Y.V.L. Ravikumar, S. Sridhar, S.V. Satyanarayana, Development of an electrodialysis-distillation integrated process for separation of hazardous sodium azide to recover valuable DMSO solvent from pharmaceutical effluent, *Sep. Purif. Technol.* 110 (2013) 20–30, <https://doi.org/10.1016/j.seppur.2013.02.031>.
- [22] E. Vera, J. Ruales, M. Dornier, J. Sandeaux, R. Sandeaux, G. Pourcelly, Deacidification of clarified passion fruit juice using different configurations of electrodialysis, *J. Chem. Technol. Biotechnol.* 78 (2003) 918–925, <https://doi.org/10.1002/jctb.827>.
- [23] K.G. Nayar, P. Sundararaman, C.L. O'Connor, J.D. Schacherl, M.L. Heath, M. O. Gabriel, S.R. Shah, N.C. Wright, A.G. Winter, V. feasibility study of an electrodialysis system for in-home water desalination in urban India, *Dev. Eng.* 2 (2016) 38–46, <https://doi.org/10.1016/j.deveng.2016.12.001>.
- [24] M. Sadrzadeh, T. Mohammadi, Sea water desalination using electrodialysis, *Desalination* 221 (2008) 440–447, <https://doi.org/10.1016/J.DESAL.2007.01.103>.
- [25] G. Doornbusch, H. Swart, M. Tedesco, J. Post, Z. Borneman, K. Nijmeijer, Current utilization in electrodialysis: electrode segmentation as alternative for multistaging, *Desalination* 480 (2020), 114243, <https://doi.org/10.1016/j.desal.2019.114243>.
- [26] M. Sadrzadeh, A. Razmi, T. Mohammadi, Separation of different ions from wastewater at various operating conditions using electrodialysis, *Sep. Purif. Technol.* 54 (2007) 147–156, <https://doi.org/10.1016/j.seppur.2006.08.023>.
- [27] A.H. Galama, G. Daubaras, O.S. Burheim, H.H.M. Rijnaarts, J.W. Post, Seawater electrodialysis with preferential removal of divalent ions, *J. Memb. Sci.* 452 (2014) 219–228, <https://doi.org/10.1016/j.memsci.2013.10.050>.
- [28] Y. Zhang, S. Paepen, L. Pinoy, B. Meessaert, B. Van Der Bruggen, Selectrodialysis: fractionation of divalent ions from monovalent ions in a novel electrodialysis stack, *Sep. Purif. Technol.* 88 (2012) 191–201, <https://doi.org/10.1016/j.seppur.2011.12.017>.
- [29] B. Cohen, N. Lazarovitch, J. Gilron, Upgrading groundwater for irrigation using monovalent selective electrodialysis, *Desalination* 431 (2018) 126–139, <https://doi.org/10.1016/j.desal.2017.10.030>.
- [30] Z. Qian, H. Miedema, S. Sahin, L.C.P.M. de Smet, E.J.R. Sudhölter, Separation of alkali metal cations by a supported liquid membrane (SLM) operating under electro dialysis (ED) conditions, *Desalination* 495 (2020), 114631, <https://doi.org/10.1016/j.desal.2020.114631>.
- [31] N.M. Kocherginsky, Q. Yang, L. Seelam, Recent advances in supported liquid membrane technology, *Sep. Purif. Technol.* 53 (2007) 171–177, <https://doi.org/10.1016/j.seppur.2006.06.022>.
- [32] A. Šlampová, P. Kubán, P. Boček, Fine-tuning of electromembrane extraction selectivity using 18-crown-6 ethers as supported liquid membrane modifiers, *Electrophoresis* 35 (2014) 3317–3320, <https://doi.org/10.1002/elps.201400372>.

- [33] P.K. Parhi, Supported liquid membrane principle and its practices: a short review, *J. Chem.* (2013), <https://doi.org/10.1155/2013/618236>.
- [34] Y. Asensio C.M. Fernandez-Marchante J. Lobato P. Cañizares M.A. Rodrigo, Influence of the ion-exchange membrane on the performance of double-compartment microbial fuel cells, (n.d.).
- [35] Jingwei Zhou, Han Kuang, Wei Zhuang, Yong Chen, Dong Liu, Hanjie Ying, Wu. Jinglan, Application of electro dialysis to extract 5'-ribonucleotides from hydrolysate: efficient decolorization and membrane fouling, *RSC Adv.* 8 (2018) 29115–29128, <https://doi.org/10.1039/C8RA02550A>.
- [36] S. Sahin, J.E. Dykstra, H. Zuilhof, R.L. Zornitta, L.C.P.M. De Smet, Modification of cation-exchange membranes with polyelectrolyte multilayers to tune ion selectivity in capacitive deionization, *ACS Appl. Mater. Interfaces* 12 (2020) 34746–34754, <https://doi.org/10.1021/ACSAMI.0C05664>.
- [37] T. Sata, R. Izuo, Modification of the transport properties of ion exchange membranes. XII. Ionic composition in cation exchange membranes with and without a cationic polyelectrolyte layer at equilibrium and during electro dialysis, *J. Membr. Sci.* 45 (1989) 209–224, [https://doi.org/10.1016/S0376-7388\(00\)80515-3](https://doi.org/10.1016/S0376-7388(00)80515-3).
- [38] G. Saracco, Transport properties of monovalent-ion-permselective membranes, *Chem. Eng. Sci.* 52 (1997) 3019–3031, [https://doi.org/10.1016/S0009-2509\(97\)00107-3](https://doi.org/10.1016/S0009-2509(97)00107-3).
- [39] B.A. Cooke, Concentration polarization in electro dialysis-I. The electrometric measurement of interfacial concentration, *Electrochim. Acta* 3 (1961) 307–317, [https://doi.org/10.1016/0013-4686\(61\)85007-X](https://doi.org/10.1016/0013-4686(61)85007-X).
- [40] I. Rubinstein, Theory of concentration polarization effects in electro dialysis on counter-ion selectivity of ion-exchange membranes with differing counter-ion distribution coefficients, *J. Chem. Soc. Faraday Trans.* 86 (1990) 1857–1861, <https://doi.org/10.1039/FT9908601857>.
- [41] X. Xiao, M.A. Shehzad, A. Yasmin, Z. Ge, X. Liang, F. Sheng, W. Ji, X. Ge, L. Wu, T. Xu, Anion permselective membranes with chemically-bound carboxylic polymer layer for fast anion separation, *J. Membr. Sci.* 614 (2020), <https://doi.org/10.1016/j.memsci.2020.118553>.
- [42] J.C. de Valenca, Overlimiting Current Properties at Ion Exchange Membranes, University of Twente, 2017, <https://doi.org/10.3990/1.9789036543149>.
- [43] A. Uzdanova, M. Urtenov, Potentiodynamic and galvanodynamic regimes of mass transfer in flow-through electro dialysis membrane systems: numerical simulation of electroconvection and current-voltage curve, *Membranes (Basel)* 10 (2020), <https://doi.org/10.3390/membranes10030049>.
- [44] Z. Qian, H. Miedema, L.C.P.M. de Smet, E.J.R. Sudhölter, Permeation selectivity in the electro-dialysis of mono- and divalent cations using supported liquid membranes, *Desalination* 521 (2022), 115398, <https://doi.org/10.1016/j.desal.2021.115398>.
- [45] Y.D. Ahdab, D. Rehman, G. Schücking, M. Barbosa, V. John, H. Lienhard, Treating irrigation water using high-performance membranes for monovalent selective electro dialysis, *ACS ES&T Water* 1 (2020) 117–124, <https://doi.org/10.1021/ACSESTWATER.0C00012>.
- [46] T. Sata, Theory of membrane phenomena in ion exchange membranes, in: *Ion Exch. Membr.*, Royal Society of Chemistry, 2007, pp. 7–34, <https://doi.org/10.1039/9781847551177-00007>.
- [47] Y. Tanaka, Fundamental properties of ion exchange membranes, in: *Ion Exch. Membr.*, Elsevier, 2015, pp. 29–65, <https://doi.org/10.1016/b978-0-444-63319-4.00002-x>.
- [48] B. Tansel, Significance of thermodynamic and physical characteristics on permeation of ions during membrane separation: hydrated radius, hydration free energy and viscous effects, *Sep. Purif. Technol.* 86 (2012) 119–126, <https://doi.org/10.1016/j.seppur.2011.10.033>.
- [49] L. Ge, B. Wu, D. Yu, A.N. Mondal, L. Hou, N.U. Afsar, Q. Li, T. Xu, J. Miao, T. Xu, Monovalent cation perm-selective membranes (MCPMS): New developments and perspectives, *Chin. J. Chem. Eng.* 25 (2017) 1606–1615, <https://doi.org/10.1016/j.cjche.2017.06.002>.
- [50] T. Sata, T. Sata, W. Yang, Studies on cation-exchange membranes having permselectivity between cations in electro dialysis, *J. Membr. Sci.* 206 (2002) 31–60, [https://doi.org/10.1016/S0376-7388\(01\)00491-4](https://doi.org/10.1016/S0376-7388(01)00491-4).
- [51] T. Luo, F. Roghman, M. Wessling, Ion mobility and partition determine the counter-ion selectivity of ion exchange membranes, *J. Membr. Sci.* 597 (2020), 117645, <https://doi.org/10.1016/j.memsci.2019.117645>.
- [52] T. Luo, S. Abdu, M. Wessling, Selectivity of ion exchange membranes: a review, *J. Membr. Sci.* 555 (2018) 429–454, <https://doi.org/10.1016/j.memsci.2018.03.051>.
- [53] I. Stenina, D. Golubenko, V. Nikonenko, A. Yaroslavtsev, Selectivity of transport processes in ion-exchange membranes: relationship with the structure and methods for its improvement, *Int. J. Mol. Sci.* 21 (2020) 1–33, <https://doi.org/10.3390/ijms21155517>.
- [54] I.A. Stenina, A.B. Yaroslavtsev, Ionic mobility in ion-exchange membranes, *Membranes (Basel)* 11 (2021), <https://doi.org/10.3390/membranes11030198>.
- [55] K.J. Kim, M. Shahinpoor, Effective diffusivity of nanoscale ion–water clusters within ion-exchange membranes determined by a novel mechano-electrical technique, *Int. J. Hydrog. Energy* 28 (2003) 99–104, [https://doi.org/10.1016/S0360-3199\(02\)00026-5](https://doi.org/10.1016/S0360-3199(02)00026-5).
- [56] B. Hille, *Ion Channels of Excitable Membranes*, Sinauer, 2001.
- [57] H. Strathmann, Electro dialysis, a mature technology with a multitude of new applications, *Desalination* 264 (2010) 268–288, <https://doi.org/10.1016/j.desal.2010.04.069>.
- [58] M. Li, A. Ju, X. Li, M. Ge, Electrochemical determination of ionization constants of tetrabutylammonium salt in acetonitrile and o-nitrophenyloctylether, *Ionics (Kiel)* 12 (2014) 1777–1782, <https://doi.org/10.1007/S11581-014-1117-0>.